Invited paper

OPTO-ELECTRONICS REVIEW 7(3), 181–195 (1999)

Optical techniques used for *in-situ* studies of MBE growth processes

M.A. HERMAN*

Institute of Vacuum Technology and Institute of Physics PASc.,
44/50 Długa Str., 00-241 Warsaw, Poland

The principles and application possibilities of optical characterization techniques as applied to in-situ monitoring of MBE growth processes are presented and discussed in this review. Emphasis is put on comparison of the presented optical techniques with other monitoring techniques, usually used in the MBE systems (e.g., RHEED technique). An optical probe (light beam) is noninvasive and nondestructive towards thin film structures grown by MBE, penetrating into (or through) these structures and the substrate crystal. Surface sensitivity of such a probe can be estimated from the optical absorption coefficient, which in semiconductors rarely exceeds 10^6 cm^{-1} and consequently implies optical penetration depths of 100 Å or more. Consequently, the surface typically contributes only about 1% to the total optical signal. Whether or not an optical probe is surface- sensitive or bul- sensitive depends on whether or not symmetry is used to suppress the ordinarily dominant bulk contribution to the overall optical signal. Laser interferometry, reflectance difference spectroscopy, and p-polarized reflectance spectroscopy are discussed in details, as applied to in-situ control of the MBE growth processes.

Keywords: optical characterization techniques, molecular beam epitaxy, surface structures

1. Introduction

Molecular Beam Epitaxy (MBE) is a versatile technique for growing thin epitaxial structures made of semiconductors, metals or insulators [1]. In MBE, thin films crystallise via reactions between thermal-energy molecular or atomic beams of the constituent elements and a substrate surface which is maintained at an elevated temperature in ultrahigh vacuum (UHV). The composition of the grown epilayer and its doping level depend on the relative arrival rates of the constituent elements and dopants, which in turn depend on the evaporation rates of the appropriate sources. The growth rate of typically 1 μm/h (1 monolayer/s) is low enough that surface migration of the impinging species on the growing surface is ensured. Consequently, the surface of the grown film is very smooth. Simple mechanical shutters in front of the beam sources are used to interrupt the beam fluxes, i.e., to start and to stop the deposition and doping. Changes in composition and doping can thus be abrupt on an atomic scale.

MBE is, by definition, an epitaxial growth process. Epitaxy means a growth process of a solid film on a crystalline substrate, in which the atoms of the growing film mimic the arrangement of the atoms of the substrate crystal. Consequently, the layer grown epitaxially should exhibit: (i) the same crystal structure, and (ii) the same crystallographic orientation as the substrate. This is true for homoepitaxy (the epilayer and the substrate are identical materials) and so-called soft heteroepitaxy when the epilayer and the substrate are two different materials lattice-matched like, e.g., GaAs and AlGaAs, or CdTe and HgCdTe, material systems. However, when the epilayer to be grown is strongly different from the substrate by at least one of the following parameters: lattice constant, crystal structure, nature of the chemical bonds, then the so-called hard heteroepitaxy occurs [2]. Neither the crystallographic orientation of the epilayer can easily be predicted in this case, nor can simple solutions be given a priori to problems that arise usually during such growth processes. Let us mention only two of these problems: (a) how one can get a certain surface orientation by choosing suitable growth con-

* e-mail: herman@alpha1.ifpan.edu.pl

ditions if different surface orientations may grow, as for instance in the case of the CdTe/GaAs (100) interface [3], (b) what is the volume fraction of each of the orientations occurring in the epilayer if different orientations grow simultaneously.

Epitaxial growth in MBE is realised on the surface of a monocrystalline substrate. A series of surface processes are involved in MBE growth, however, the following are the most important: (i) adsorption of the constituent atoms or molecules impinging on the substrate surface, (ii) surface migration and dissociation of the adsorbed molecules, (iii) incorporation of the constituent atoms into the crystal lattice of the growing epilayer, and (iv) thermal desorption of the species not incorporated into the crystal lattice. These processes are schematically illustrated in Fig.1, where the substrate crystal surface is divided into so-called crystal sites with which the impinging molecules or atoms may interact. Each crystal site is a small part of the crystal surface characterized by its individual chemical activity. A site may be created by a dangling bond, vacancy, step edge, etc. [4].

In MBE, most frequently the reflection high-energy electron diffraction (RHEED) technique is used for *in-situ* probing of the surface kinetic processes [5]. The experimental geometry of the RHEED system is illustrated schematically in Fig. 2. Electrons having energy of typically 10-20 keV are incident on the substrate at a glancing angle ($0 \leq \Theta \leq 5°$). The diffraction of the incoming primary beam leads to the appearance of intensity-modulated streaks (or rods) normal to the shadow edge superposed on a fairly uniform background which is due to inelastically scattered electrons. The information which may be gained by RHEED in MBE is sufficiently complete, that nearly perfect control of the growth process is possible. The static mode of RHEED (no growth occurs) delivers information on crystallinity and lattice constant, as well as on surface reconstruction and morphology of the epilayer's surface. The dynamic mode of RHEED (growth of the epilayer proceeds) enables growth rate determination and control. It gives also chemical composition of the film and enables beam flux calibration. Looking at Fig. 2, one may recognise why the geometry of the RHEED system is ideal for combination with MBE, where it is desirable to have the molecular beams impinging on the substrate surface at near-normal incidence [1].

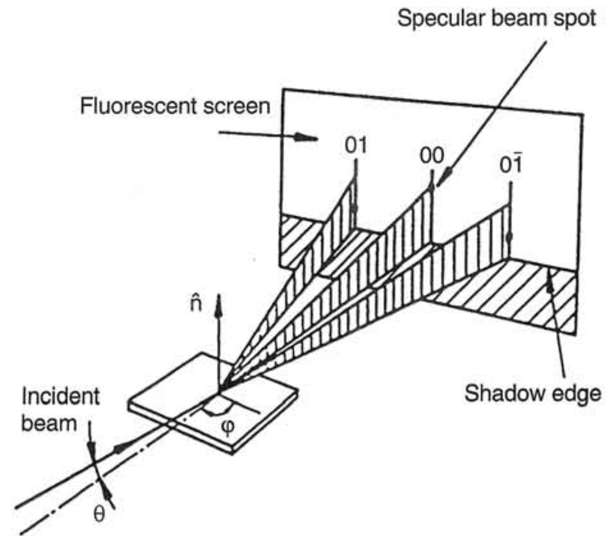

Fig. 2. Schematic illustration of the RHEED system geometry showing the incident beam at an angle θ to the surface plane and an azimuthal angle φ. The elongated spots indicate the intersection of the Ewald sphere with the 01, 00, and 0$\bar{1}$ rods (after Ref. 1).

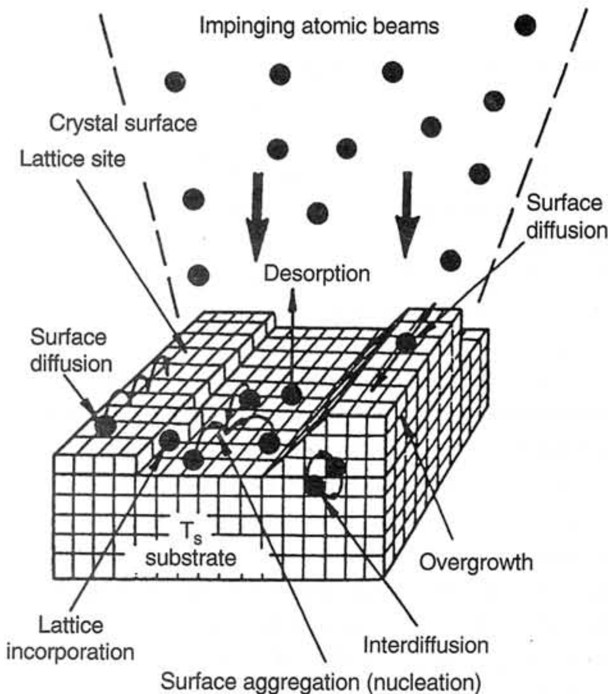

Fig. 1. Schematic illustration of the surface processes occurring during film growth by MBE (after Ref. 1).

In the recent decade, an enormous progress of optical surface analysis techniques has been observed [6], from which also MBE growth technique has benefited a lot [1]. First of all optical techniques are nondestructive and their sensitivity has been improved to such extend that nowadays the surface analysis can be performed *in-situ* on epilayers with thicknesses on the atomic scale. Spatial and temporal resolution of these techniques have been pushed to the limits

 © 1999 COSiW SEP, Warsaw

which enable real time observation of surface processes during MBE growth. Optical techniques complement the RHEED technique in MBE technology, however, they are apparently moving only slowly into this growth technique. One reason for this might be the two disadvantages exhibited by optical techniques, i.e., a limited spectral range, and the low surface contribution to the total optical signal related to the analysed epilayer(s)/substrate system, estimated to be equal only to about 1%. Because of the relatively weak interaction between photons and their surroundings, a specularly reflected optical beam will have sampled a significant amount of bulk material in addition to the surface. Consequently, an optical probe returns information from the whole penetration depth, thus, it delivers direct information on composition of the epilayer and on its thickness as well. Whether or not an optical probe is surface- or bulk- sensitive depends on whether or not symmetry is used to suppress the ordinarily dominant bulk contribution to the optical signal.

This review is aimed at giving current information on the status of optical techniques with respect to the analysis of thin semiconductor epilayers during their growth by MBE. Laser interferometry, reflectance difference spectroscopy (called also reflectance anisotropy spectroscopy), and p-polarized reflectance spectroscopy are discussed in details.

2. Laser interferometry

Using laser interferometry (LI), laser light of a wavelength λ which is mostly transparent to the substrate (deposited film) illuminates the substrate (film) at a small incidence angle α_i ($\approx 1°$). Combination of light reflecting from the top surface of the substrate (film) with the light transmitted through the substrate (film) and reflected off the polished back surface of the substrate (the film-substrate interface) causes so-called multiple beam interference [7]. The intensity of reflected light oscillates in a periodic fashion with increasing temperature or layer thickness as the optical pathlength within the substrate (film) increases, because of the increase in n and d. One full cycle in the observed reflection-interference oscillations, i.e., in the “interferogram” [8] corresponds to an increase (decrease) in the optical pathlength of $\lambda/2n$ at normal incidence.

Let us consider a plane-parallel wafer of medium (r) sandwiched between two media (i) and (s) with different refractive indices n_i and n_s (Fig. 3). Let the electromagnetic wave of the laser incident on this wa-

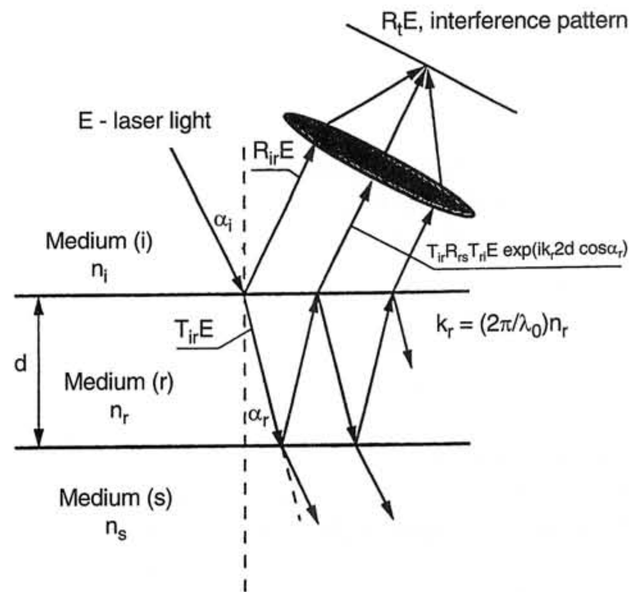

Fig. 3. Schematic illustration of the reflection of a laser light wave in a plane-parallel wafer of the medium r sandwiched between the medium i and s, respectively, with the refractive indices different from n_r. The multiple-beam interference pattern is formed in the focus plane of the lens (after Ref. 7).

fer from the side of medium (i) be represented by an electric field plane wave $E(r,t) = E_0 \exp[i(\omega t - kr)]$, with $\omega = 2\pi f$, $k = 2\pi n/\lambda_0$, E_0, r and t having the meaning of the angular frequency, wave number, electric field amplitude, spatial coordinate and time, respectively. n, f and λ_0 have the usual meaning, namely, the refractive index, frequency and wavelength in vacuum.

When crossing an interface, e.g., the (i)/(r) interface, this wave will be divided into the reflected wave $R_{ir}E$ and the transmitted wave $T_{ir}E$. The reflection and transmission coefficients may be evaluated from Fresnel formulae [8]

$$R_{ir} = \frac{\sin(\alpha_r - \alpha_i)}{\sin(\alpha_r + \alpha_i)} \tag{1}$$

$$T_{ir} = \frac{2\sin\alpha_r \cos\alpha_i}{\sin(\alpha_r + \alpha_i)} \tag{2}$$

where α_i and α_r are the incidence and the refraction angles, respectively (Fig. 3). Using Snell's law $n_i \sin\alpha_i = n_r \sin\alpha_r$, one may write the formulae in the form

$$R_{ir} = \frac{n_i - n_r}{n_i + n_r} \tag{3}$$

$$T_{ir} = \frac{2n_i}{n_i + n_r} \quad (4)$$

The total intensity of the reflected light incident onto the lens shown in Fig. 3 may be evaluated by summing up the intensities of the constituent beams reflected up and down at the surfaces of the wafer. The general formula

$$R_t E = R_{ir} E + T_{ir} R_{rs} T_{ri} E \exp(ik_r 2d \cos\alpha_r) + T_{ir} R_{ri} R_{rs} T_{ri} E \exp(ik_r 4d \cos\alpha_r) + \ldots \quad (5)$$

indicates that for each constituent beam of the reflected light the variable part of the phase of the wave E, differs from that of the preceeding beam by an amount Δ, which corresponds to a double transversal of the wafer. Considering the geometry of the "wafer-light beams" system shown in Fig. 3 and using Snell's law one may calculate that

$$\Delta = 2k_r d \cos a_r = (4\pi/\lambda_0) n_r d \cos\alpha_r. \quad (6)$$

Assuming, for simplicity, that $n_s = n_i$, one may put $R_{rs} = R_{ri}$, which considerably simplifies formula (5). Taking now into account that the intensity of light is given by the squared absolute value of the amplitude of the light wave, one gets for the intensity of the total reflected light a simple formula

$$I_R = C(1 - \cos\Delta). \quad (7)$$

The constant C is real, and it depends on the reflection coefficient R_{ri} of the considered plane-parallel wafer and on the intensity of the incident light [7]. One may now conclude that the total intensity of the light reflected from the wafer is a cosine function of the thickness and the refractive index of the wafer, and thus, of the temperature of the wafer. I_R = max if $\Delta = 2\pi(m+1/2)$, while I_R = min if $\Delta = 2\pi m$, where m is an integer. It should be pointed out that this general conclusion is also valid for the case when $n_s \neq n_i$ [9].

2.1. Laser interferometric thermometry

Optical interferometry, in its variant called laser interferometric thermometry (LIT), may be used for exact determination of growth temperature in MBE systems. In the MBE growth technique infrared pyrometers may be used for direct measurement of the substrate temperature by viewing the substrate through a viewport, thus allowing calibration of the manipulator thermocouple. However, when there are light reflections from the substrate surface originating from a light source on the same side of the surface as the pyrometer, then the substrate temperature cannot be reliably measured with a pyrometer; this happens, for example, during MBE growth when an effusion cell of the MBE system is open (the glowing crucible of the cell is the light source). In order to avoid this difficulty one may use the LIT technique [7] for exact calibration of the manipulator's thermocouple, and thus, for exact determination of the real temperature of the substrate in the MBE system.

When the LIT technique is applied to semiconductors, an important simplification may be introduced which is justified by the characteristic feature of these materials, namely, a much greater sensitivity to temperature of the refractive index n than of the thickness d of the substrate wafers or grown films [7]. Consequently, one may ignore the influence of the thermal dependence of d on the optical pathlength in the first approximation of the evaluations required in this technique.

In order to get reliable values of the substrate (film) temperature, the "interferograms" related to the changes of the substrate temperature need to be calibrated in temperature values, i.e., temperatures should be ascribed to the sequential maxima (minima) numbers of the "interferogram". This calibration procedure should be performed in thermally steady-state conditions. Under these, one understands usually conditions at which temperature changes occurring during heating-up or cooling-down processes in the calibration procedure are so slow that no changes in the "interferogram" can be recorded when the temperature scan is interrupted.

Let us consider as an example the calibration procedure performed in [Ref. 7] for a GaP substrate wafer. The set-up of the calibration system is shown in Fig. 4. The GaP wafer is placed in a specially designed sample holder made of copper. A uniform temperature distribution over the whole wafer and the measuring thermocouple is ensured by the construction of the holder and Cu-tube in the furnace. The thermocouple is dipped in a heat conducting Ga-In mixture which is in direct contact with the bottom surface of the wafer. The upper surface of the wafer is in contact with the holder lid which has an opening, 3.8 mm in diameter, in its central part allowing the incidence on, and reflection from, the wafer surface of the laser light. During the calibration procedure, the sample holder is positioned in the central part of the furnace, 630 mm long, in the quartz-glass tube which

 © 1999 COSiW SEP, Warsaw

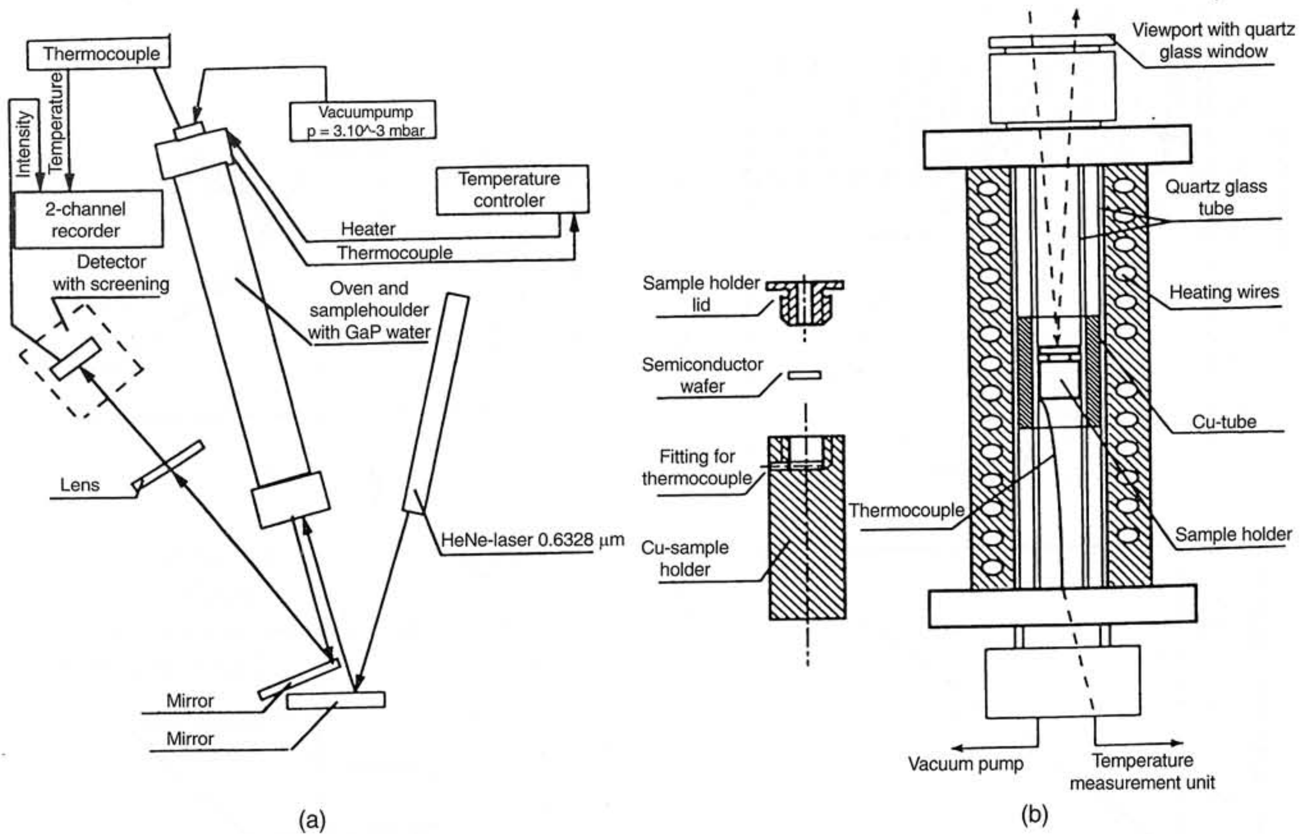

Fig. 4. (a) Set-up of the system used for calibration of the GaP wafer "interferogram" and (b) schematic illustration of the construction of the furnace and the sample holder of the system (after Ref. 7).

is surrounded in its middle part by an additional Cu-tube, as shown in Fig. 4(b); this ensures a homogeneous temperature distribution over the whole length of the sample holder. In the quartz-glass tube a vacuum of about 10^{-1} mbar is generated by an external pumping unit, what protects the upper surface of the GaP wafer from being contaminated by gas layer which could eventually influence the optical properties of the wafer during the calibration procedure. The He-Ne laser light of 0.6326 μm wavelength enters the quartz-glass tube through a vacuum-tight viewport with a quartz-glass window. After being reflected from the GaP wafer, the laser light coming out through the viewport is directed by a simple optical system on the Si photodiode placed in a dark housing [Fig. 4(a)]. The electrical current generated by the photodiode, when illuminated by the reflected laser beam, and the thermoelectric voltage from the thermocouple, indicating the temperature of the GaP wafer, are simultaneously recorded by a 2-channel X–Y plotter. Thus, a temperature calibration curve for the oscillations is plotted over the "interferogram" curve. In that way, each maximum could be attributed to a certain temperature. An exemplary diagram of the two overlapping curves measured whilst cooling-down the furnace (and thus the GaP wafer) with a rate of 1.7°C min^{-1} is shown in Fig. 5(a), and the relevant calibration curve for the wafer temperature is shown in Fig. 5(b).

Having calibrated the "interferogram" in temperature values, one may now proceed to calibration of the MBE manipulator thermocouple. Depending on the geometry of the substrate heating and thermocouple (SHT) system in a definite MBE deposition chamber, the temperature of the substrate wafer, indicated by the manipulator thermocouple differs more or less from the real temperature of the substrate wafer [9]. For the manipulator thermocouple calibration procedure, the GaP wafer fixed to the substrate holder, as shown in Fig. 6(b), has been heated-up in a vacuum of 10^{-8} mbar to the temperature of 400°C, according to the indications of the thermocouple. After 1 hour since this moment the thermocouple indication became constant at the level of 400°C; the "interferogram" curve of the GaP wafer remained unchanged, too. Consequently, it could be concluded that the sample holder exhibited a constant temperature at that moment. Subsequently, a slow cooling-down process, according to the program shown in Fig. 6(a), was started. This program, with cooling rates of 1°C min^{-1}

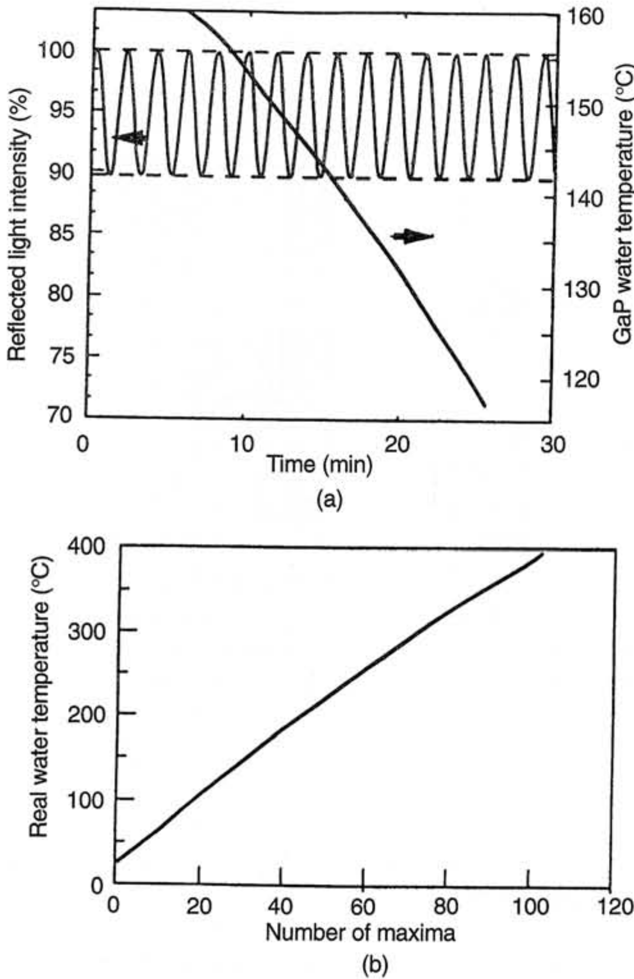

Fig. 5. (a) Example of an "interferogram" of the GaP wafer with the overlapping temperature calibration curve, recorded during the cooling-down process of the wafer from 160°C to 120°C with a rate equal to 1.7°C min^{-1}, and (b) the relevant complete temperature calibration curve plotted according to the numerical data given in Table1 (after Ref. 7).

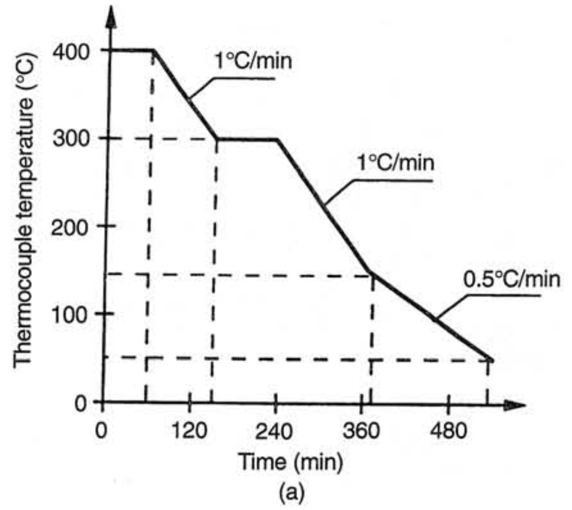

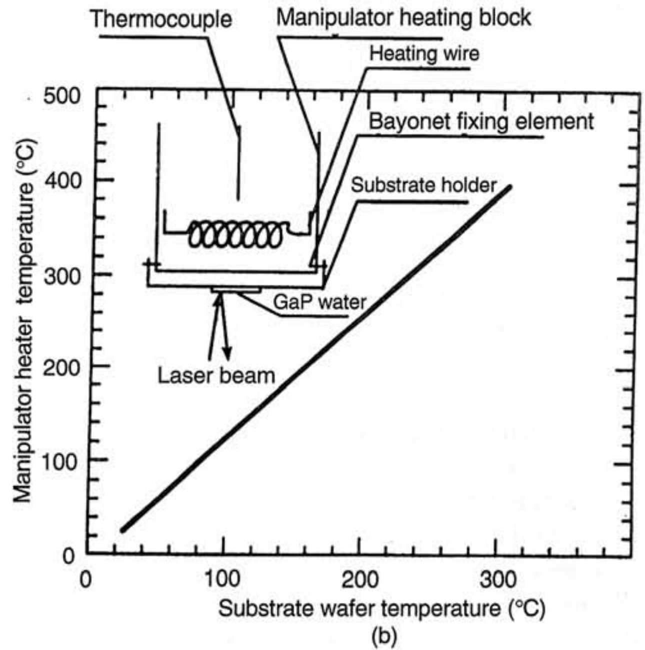

Fig. 6. (a) The cooling-down program of the heating block of the manipulator (according to the thermocouple indications) which ensures thermal steady-state conditions during the calibration procedure, and (b) the manipulator thermocouple calibration curve. The geometry of the SHT system is shown schematically in the inset (after Ref. 7).

and 0.5°C min^{-1}, ensured thermal steady-state conditions in the SHT system, which has been confirmed experimentally. When the cooling process was interrupted for 10 min at 300°C, no changes in the "interferogram" were observed in that time interval. During the programmed cooling-down process the thermocouple indications (the as-measured temperatures) and the reflected laser light intensity oscillations (the GaP wafer "interferogram") were simultaneously recorded by a 2-channel X–Y plotter. The real substrate temperatures could then be determined from the "interferogram" maxima by assuming that the final temperature of the cooling process, i.e., 25°C (the room temperature), indicated by the thermocouple was equal to the real substrate temperature. Counting back the interference maxima, starting with number 1 for the temperature 27°C and comparing these "interference maxima GaP wafer temperatures" with the recorded indications of the thermocouple, the calibration data for the thermocouple may be evaluated. The thermocouple calibration curve is shown in Fig. 6(b).

After the calibration procedures described above have been completed, a set of experiments were performed, which concerned the thermal behaviour of the MBE system manipulator in dynamic conditions, i.e., when temperature changes are generated with fairly high heating or cooling rates. The temperature changes have been chosen to be similar to those,

 © 1999 COSiW SEP, Warsaw

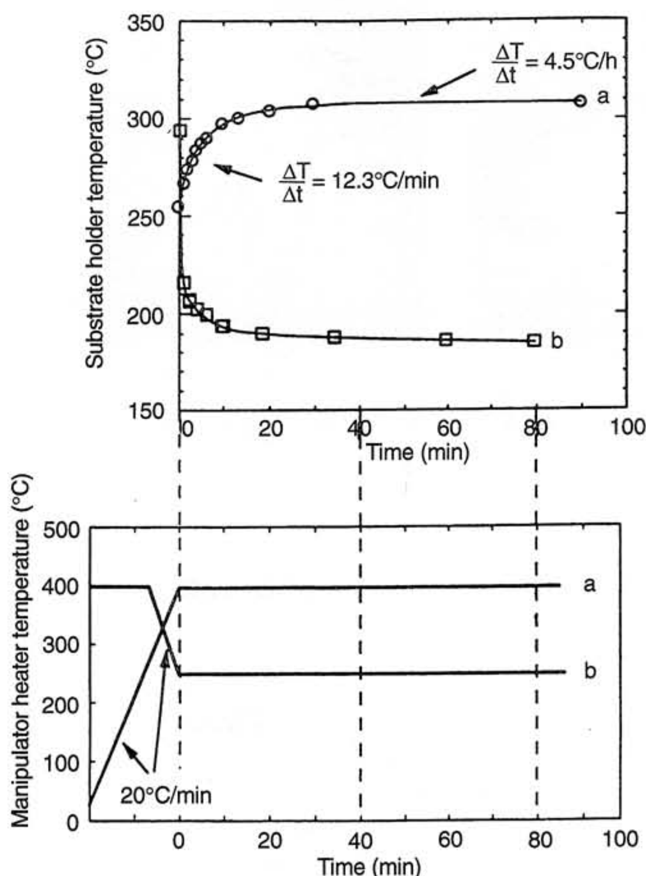

Fig. 7. (a) Changes of the substrate holder temperature after the thermocouple showed a constant temperature of 400°C after a rapid heating or (b) 250°C after a rapid cooling process (after Ref. 7).

which occur in real MBE growth processes of the wide-gap II-VI semiconductor compounds.

Figure 7 (upper panel) shows the thermal behaviour of the manipulator substrate holder (substrate wafer) after the intended temperature of 400°C has been reached, according to the thermocouple indications, when fairly short heating and cooling processes were performed (shown in the lower panel of Fig. 7). At constant thermocouple temperatures, the real wafer temperature still changed. A rising-up rate of the substrate temperature of about 12°C min^{-1} within the 20 min interval, and of about 5°C min^{-1} in the subsequent 70 min. interval, was measured by LIT. After this experiment, the heating block was cooled-down with the same rate of 20°C min^{-1}, according to the indications of the thermocouple, while simultaneously recording the real substrate temperature determined by LIT. Again a considerable delay between the thermocouple and substrate temperatures was found, as shown in Fig. 7 (upper panel).

2.2. Temperature window of the MBE growth processes

A proper adjustment of the growth temperature is the most important task for the MBE crystal grower [10]. The low-temperature limit for MBE to occur is defined by surface migration processes. Below some limiting temperature T_L the deposited film will be no more crystalline. MBE occurs near T_L when surface migration rate, multiplied by some weighting factor relevant for the density of appropriate lattice sites on the surface (of the substrate or already grown epilayer), exceeds the deposition rate [11]. The high temperature limit T_H is defined by the balance between adsorption and desorption processes, which results from the thermodynamic phase equilibria relations [12]. An example of how the temperature window of a MBE process may be determined has been presented in Ref. 10. This paper reports on simultaneous application of reflection mass spectrometry (REMS), laser interferometry (LI) and reflection high-energy electron diffraction (RHEED) measurements for determination of the sticking parameters for the constituent elements of the $Cd_{1-x}Zn_xTe$ ($0 \leq x \leq 1$) material system at MBE growth conditions. The experimental procedure of MBE temperature window determination is based (according to this example) on (i) the observation of the structural changes in the RHEED pattern taken from the epilayer surface when growing it near the low-temperature limit T_L, and (ii) on measuring the REMS signals of the relevant desorbing cation fluxes and on simultaneous recording of the LI intensity oscillation periods (determining the film growth or sublimation rates) when growing the epilayer near the high-temperature limit T_H. The experimental data concerning the determination of temperature limits T_L and T_H are shown in Fig. 8 and Fig. 9, respectively, for MBE growth of a ZnTe epilayer on 1 μm thick CdTe buffer layer deposited on GaAs(100) substrate, covered with a 3ML thick ZnTe epilayer.

At $T_{gr} = T_L$ the RHEED pattern changes from a streaky one (indicating a clear surface reconstruction of the atomically smooth surface) to a spotty one (indicating the roughness of the surface grown when the adsorbate migration becomes so small that no smooth epilayer surface can be grown by MBE). In the case of ternary compounds investigated in Ref. 10, the characteristic features of Figs. 8 and 9 do not change. However, the numerical data of REMS and LI signals are different and the surface reconstruction observed by RHEED at $T_{gr} > T_L$ is no more a clear 2×1 structure. At temperatures $T_{gr} << T_L$ polycrystalline layers are deposited

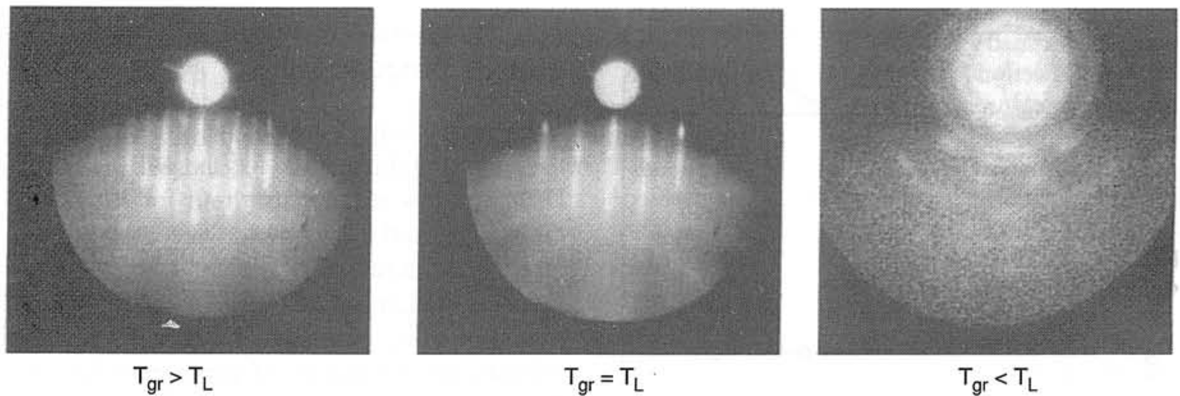

Fig. 8. RHEED patterns determining the temperature limit T_L of the MBE window for ZnTe grown on the CdTe/ZnTe(3ML)/GaAs surface, taken from the surface of an epilayer grown at $T_{gr} > T_L$ (left), $T_{gr} = T_L$ (middle) and from a polycrystalline film deposited at $T_{gr} < T_L$ (right). Tellurium 2×1 surface reconstruction is clearly shown; direction of the electron beam k ‖ $[0\ \bar{1}\ \bar{1}]$ (after Ref. 10).

(this is no more an epitaxial growth) and a relevant RHEED picture exhibiting Laue fringes is observed (see Fig. 8, right). On the other side of the MBE window, at $T_{gr} = T_H$, the epilayer growth rate measured from LI intensity oscillations [7] becomes minimal (see Fig. 9), while an increase of T_{gr} over T_H causes a decrease in LI oscillation period (increase in the sublimation rate) and a simultaneous increase in REMS signal intensity of the desorbing cation flux in the presence of the impinging anion flux. The numerical value of the MBE window for the ZnTe epilayer grown on CdTe/ZnTe(3ML)/ GaAs substrate is equal to $T_H–T_L$ = (370 – 300)°C = 70°C [10].

3. Reflectance-difference (anisotropy) spectroscopy

Reflectance-difference spectroscopy (RDS), called also reflectance-anisotropy spectroscopy (RAS) [6], relies on the fact that the surface has a lower symmetry than the bulk of an epilayer. In this technique, the difference between the near-normal-incidence reflectances of light polarized along the two principal axes of the sample in the plane of the surface (e.g., R_{110} and $R_{\bar{1}10}$) is determined experimentally [13-15]. As cubic materials are nominally isotropic, the bulk contribution essentially cancels in

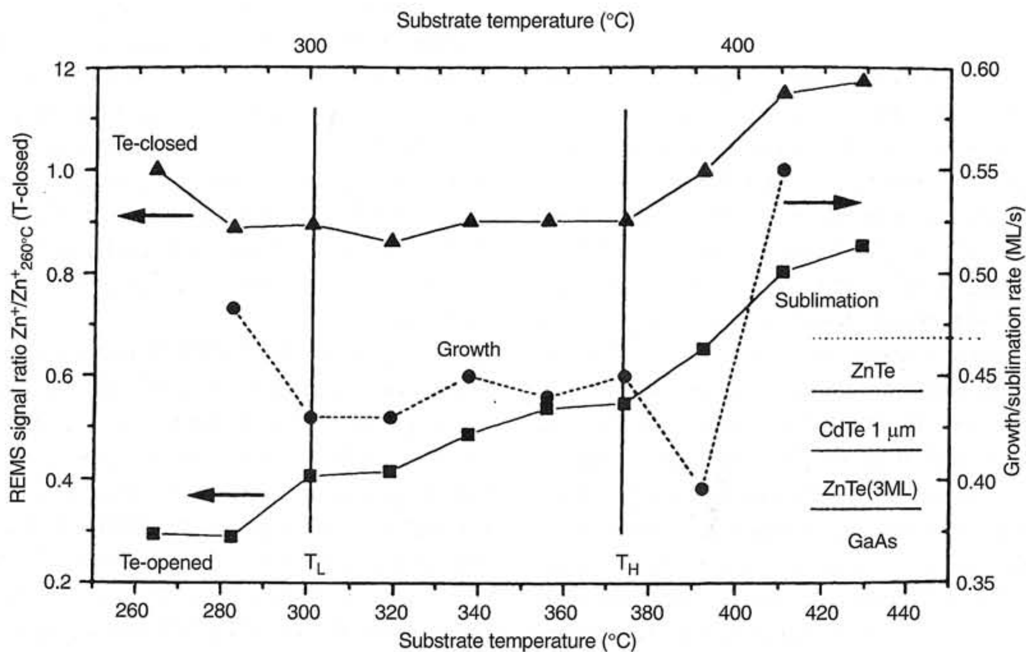

Fig. 9. The epilayer growth/sublimation rates and the normalized REMS signal intensities of the Zn^+ cation fluxes detected from ZnTe grown on the CdTe/ZnTe(3ML)/GaAs surface in the presence/absence of the Te^- anion flux impinging onto the substrate at $T_{gr} \leq T_H$ or $T_{sub} > T_H$ (after Ref. 10).

 © 1999 COSiW SEP, Warsaw

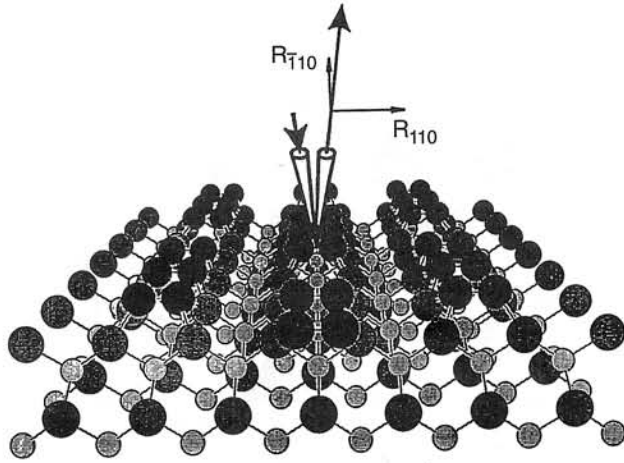

Fig. 10. Schematic set-up of RDS/RAS experimental conditions. The polarized light interacts with anisotropic electronic surface states, delivering information on: surface morphology, surface reconstruction and growth rate (after Ref. 6).

subtraction leaving only that from the lower-symmetry surface. RDS may be considered as normal-incidence ellipsometry, and as such may be used for direct optical determination of a surface dielectric response under steady-state conditions. A schematic illustration of the set-up of RDS/ RAS experiment is shown in Fig. 10. One may easily conclude, that this method: (i) is based on interaction of polarized light with anisotropic electronic surface states, and (ii) delivers information on surface morphology, surface reconstruction, and growth rate.

The principles of experimental facilities of the RDS/RAS method are most easily understood by considering the, so far, best studied example, namely the GaAs (001) surface. Figure 11 shows the two most important surface reconstructions (frequently used in MBE growth procedures) of GaAs(001) epilayers or substrate crystals, i.e., the 2×4 and the c(4×4) reconstructions [6]. Both surfaces are arsenic rich, the former containing one single As layer at the surface, while the latter contains a double layer. Both surfaces appear clearly to be anisotropic. They should, therefore, respond differently to light, since the arsenic dimers in the outermost layers of both reconstructions are oriented perpendicularly to each other. Consequently, the optical response from both surfaces, as far as the contribution from the arsenic dimers is concerned, is expected to be anisotropic and also different from each other. The reflectance contribution from such a surface with light polarized along the [110] and the [$\bar{1}$10] directions therefore should be different. The RDS signal may be written as

$$\Delta r/r = 2(r_{\bar{1}10} - r_{110})/2(r_{\bar{1}10} + r_{110}) \qquad (8)$$

or if the reflectances R = r×r* are measured, then

$$DR/R = 2(R_{\bar{1}10} - R_{110})/2(R_{\bar{1}10} + R_{110}). \qquad (9)$$

The main part of the RDS signal has been shown to arise from absorption by dimers which are a part of

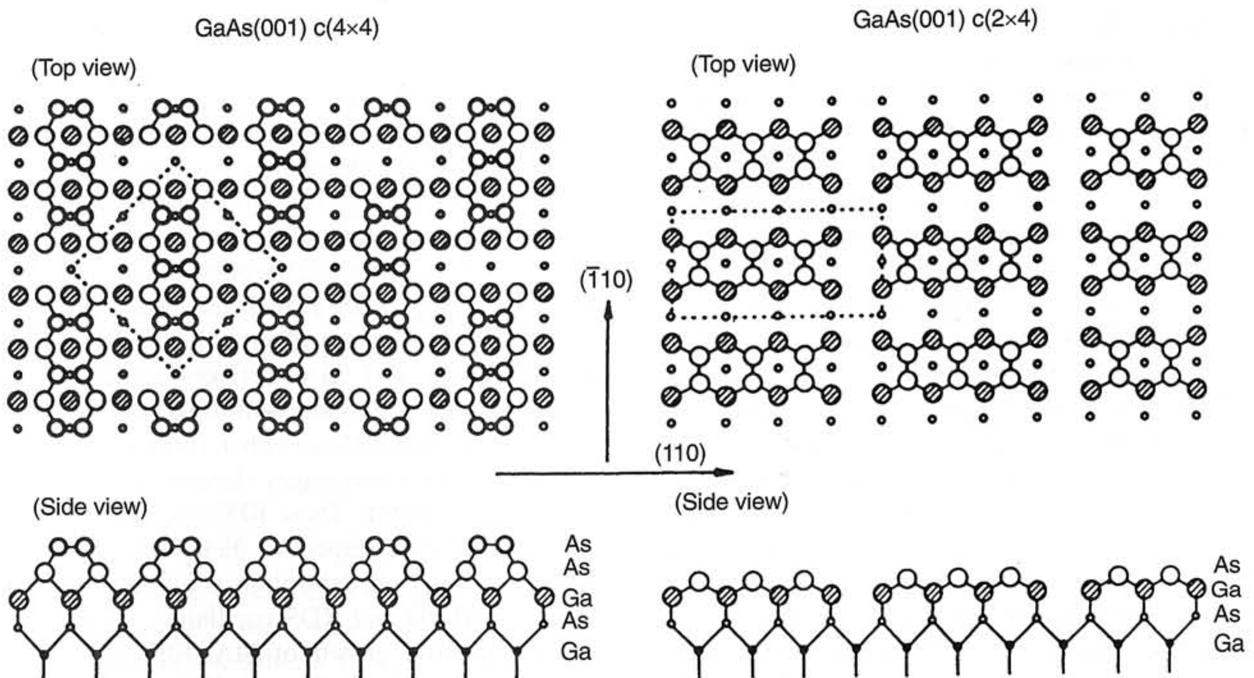

Fig. 11. Surface structure of GaAs(001) with reconstruction c(4×4), left side, and reconstruction 2×4, right side (after Ref. 6).

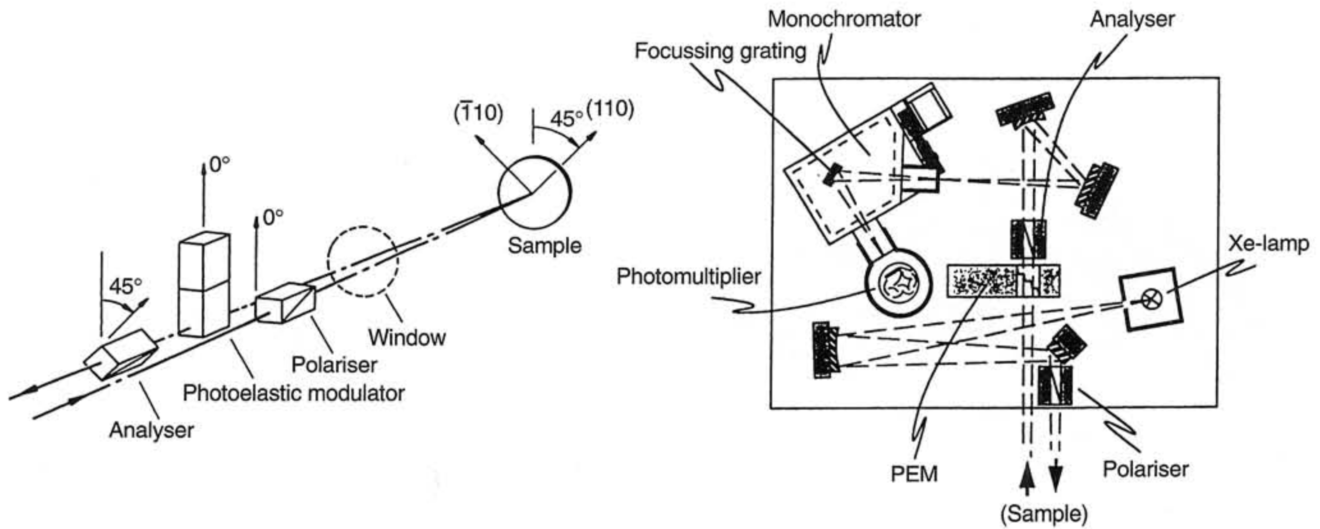

Fig. 12. (a) Principal diagram of a RDS set-up utilizing a photoelastic modulator, and (b) layout of an optical RDS spectrometer (after Ref. 6).

the surface reconstruction of the grown epilayer. This provides interesting chemical information for III-V compounds, mainly GaAs, since for this material the Ga and As dimers are oriented in the [110] and [1̄00] direction, respectively [1]. RDS can, however, also detect the geometrical structure of the surface beneath the dimer's layer if the wavelength is chosen in a region where no absorption by dimers exists. The signal is then approximately one order of magnitude smaller. The weak optical signal is usually buried in noise, however, by using a photoelastic modulator and the lock-in detecting technique, the change in polarisation state of the probe light induced by the surface may be well detected [14].

A possible realization of the experiment which allows the real as well as the imaginary part of the RDS signal to be evaluated is sketched in Fig. 12 (a). This set-up or very similar versions are now in use in several research laboratories around the world. In detail, the equipment of the photoelastic modulator (PEM) configuration consists of a 15 W Xe short-arc lamp with an accessible photon energy range from 1.5 to 6 eV, front surface focusing optics, quartz (or MgF_2) prisms, a PEM operating at 50 kHz, a short focal length grating monochromator to keep the set-up small, and an extended S20 photomultiplier [Fig. 12(b)]. The RDS signal is then extracted using a phase sensitive lock-in amplifier. A typical RDS spectrum can be recorded in a few minutes [6]. Thus, at present real-time monitoring of growth is hardly feasible utilising the full spectral range. This problem can be overcome in principle by the use of optical multichannel analyzers. Presently, the detection of changes in the RDS signal at fixed photon energy can be performed within 100 ms or less [6]. Consequently, RDS spectra taken over the entire photon energy range can be employed in order to identify the photon energies for which maximum changes occur during the growth at fixed photon energies. More details on application possibilities of RDS to epitaxial growth control can be found in Ref. 6.

Optical-reflectance and reflectance-difference changes resulting from abrupt changes in the As and Ga fluxes impinging on the GaAs(001) substrate surface during MBE growth provide surface chemical information on the growing film [16]. Thereby, these characterization techniques may be considered as complementing the structural data available from RHEED measurements.

The observed polarization and spectral dependences of the reflected optical signals [16] suggest that the optical anisotropies of the surface properties occurring during epitaxial growth arise from optical absorption associated with Ga-Ga surface dimer bonds. Another interesting property of the RDS signal occurring during MBE growth has been observed in Ref. 17. Upon initiation of growth, the RDS signals for (001) GaAs and AlAs surfaces exhibit a cyclic component that is periodic with (001) atomic bilayer coverage and that follows either surface structure or surface chemistry (coverage), depending on the measurement wavelength. These RDS oscillations may be phase shifted with respect to their RHEED counterparts, depending on deposition conditions [17]. The relevant RHEED and RDS oscillating signals corresponding to MBE growth of AlAs film on AlAs substrate, and of GaAs film on GaAs substrate, are shown in Figs. 13(a) and (b), respectively.

 © 1999 COSiW SEP, Warsaw

4. P-polarized light reflectance spectroscopy

When p-polarized light irradiates the surface of a growing film, the reflected light intensity can be minimized by setting the incidence angle close to the Brewster angle (the angle of polarization by reflection). The residual reflected light intensity observed around the Brewster angle is caused by optical absorption of the incident light at the film surface [this is the reason why the p-polarized light reflectance spectroscopy (PRS) is often called surface photo-absorption (SPA) method]. Thus, the deposition of an absorbing thin film on the substrate crystal can be easily detected by measuring the amount of light reflected from the deposited film [18-20]. The relative reflectivity change, which occurs then, can be expressed by

$$\Delta R/R = [R(d) - R(0)]/R(0) \qquad (10)$$

where R(0) and R(d) represent the reflectivity of the substrate before and after the deposition of a film of thickness d, respectively. Unlike the RDS, where the E vector of the incident light is parallel to the substrate surface, the E vector in the PRS is perpendicular to the substrate surface. The difference in studies of the surface properties during the growth when using RDS and PRS was analyzed in Ref. 18, on the example of the GaAs (001) surfaces, the Ga-stabilized and the As stabilized, respectively. For this case the measured quantity $\Delta R/R_{As}$, defined as being equal to $(R_{Ga} - R_{As})/R_{As}$, where R_{Ga} and R_{As} are the reflection coefficients for the Ga- and As-stabilized surfaces, respectively. Figure 14 shows $\Delta R/R_{As}$ plotted as a func-

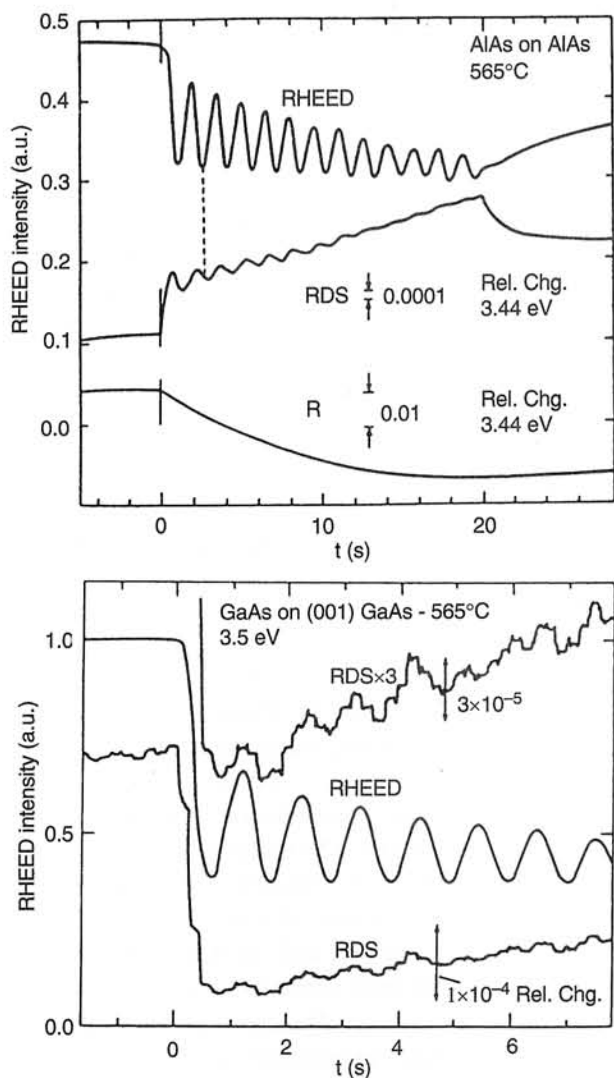

Fig. 13. (a) Averages of nine RHEED (upper curve), RDS (middle curve), and R (lower curve) signals upon initiation of AlAs growth by MBE at 1.5 s per Al monolayer (ML) on an AlAs surface, and (b) averages of 33 RHEED (middle curve) and RDS (upper, lower curves) signals upon initiation of GaAs growth by MBE at 1.1 s per Ga ML on a GaAs surface. The upper and lower curves are the same RDS data shown with different scaling factors (after Ref. 17).

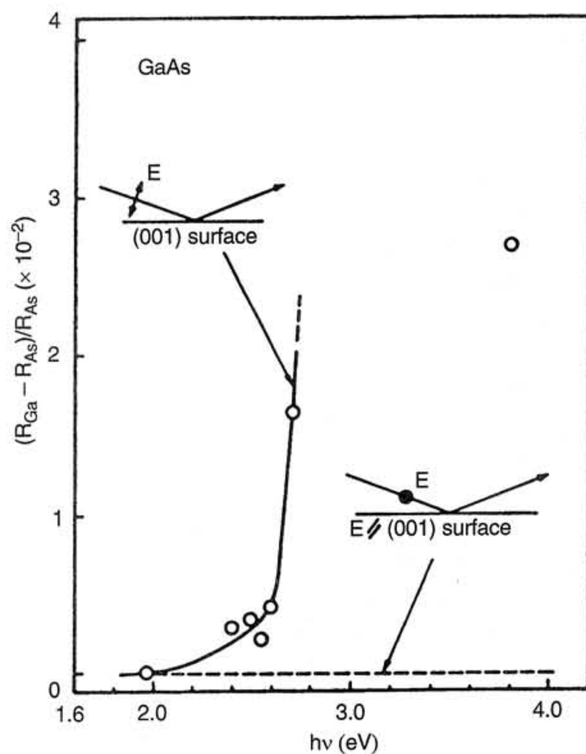

Fig. 14. Spectral dependence of $\Delta R/R_{As}$ for the GaAs(001) surface when illuminated with linearly polarized laser light of different spatial configuration of the E vector of the light wave. For E perpendicular to the surface (typical for PRS) strong dependence on photon energy of the relative reflectivity is observed, while in the case of E parallel to the surface (typical for RDS) no such dependence is observed. (after Ref. 18).

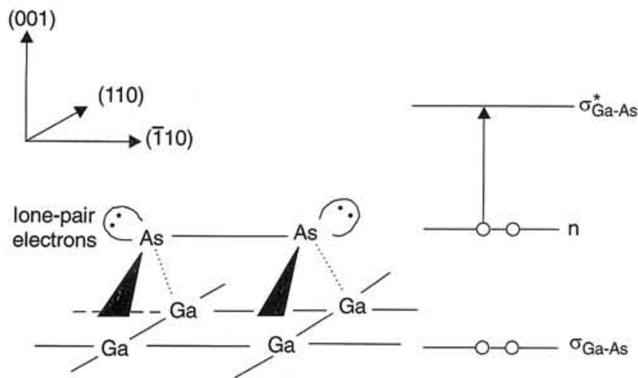

Fig. 15. As-As dimer structure formed on the GaAs(001) surface (left side) and the allowed electronic transition induced by the light with E vector perpendicular to the surface (right side) (after Ref. 18).

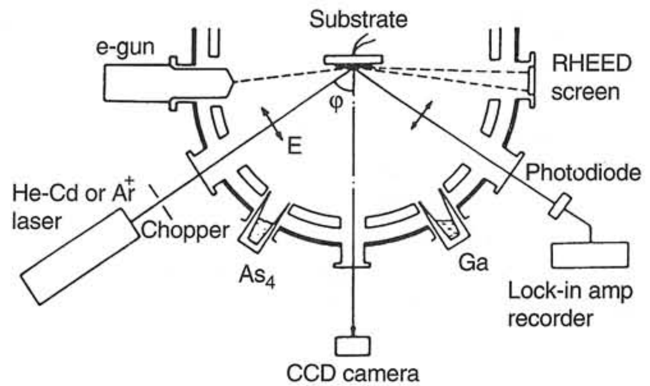

Fig. 16. Experimental setup used for the PRS method when controlling the MBE growth proccesses (after Ref. 19).

tion of the photon energy of the laser light. When a 1.959 eV He-Ne laser was used, no significant reflection change was observed between the Ga- and the As-stabilized surfaces. In the spectral range from 2.409 eV to 2.601 eV of an Ar ion laser, a small $\Delta R/R_{As}$ of less than 4×10^{-3} was observed. However, the value of $\Delta R/R_{As}$ increased rapidly when the photon energy was changed from 2.601 eV to 2.707 eV of an Ar ion laser, reaching its largest value at 3.814 eV of the He-Cd laser. In order to understand these experimental data one has to keep in mind the fact that the light absorption by the As-stabilized surface should have the electronic transition moment perpendicular to the surface. In fact, it is well known from the literature [18] that the As-stabilized GaAs(001) surface is composed of As-As dimer structures, as shown in Fig. 15. The As-As dimer structure belongs to the point symmetry group of C_{2v}. Among the allowed electronic transitions with the moment perpendicular to the surface, the transition from lone-pair electron orbitals of the As-As dimers to the surface Ga-As antibonding orbitals is the most probable in this point group. This conclusion results from the fact that the considered transition is specific to surface species having lone-pair electrons such as As-As dimers, and does not occur in either bulk GaAs or the Ga-stabilized GaAs surface, in which As atoms have no lone-pair electrons but form the sp^3 electron configuration for Ga-As bonding.

The experimental setup used for the PRS method when controlling the MBE growth process is shown in Fig. 16. It consists of a conventional MBE growth system with two quartz windows at the Brewster angle ($\varphi = 75°$), together with a RHEED diffraction system. The combination of these characterization techniques in the growth system allows for comparison of the PRS data with those obtained by RHEED observation. p-polarized laser light is used as the optical probe. It is chopped and introduced to the growth chamber as linearly polarized beam with the E-vector perpendicular to the substrate surface. The reflected light is detected with a conventional Si photodetector. The output of the detector is then routed through a lock-in amplifier and recorded on a time chart (X–Y recorder).

In order to illustrate the advantages of the PRS technique, let us describe the experimental results of Horikoshi et al. [19] concerning epitaxial growth of GaAs.

4.1. Application of PRS to MBE growth

As discussed in Ref. 18 the PRS signal increases linearly with the number of Ga atoms N_{Ga} deposited on the surface until the full coverage is accomplished ($N_{Ga} = N_s$, the number of surface sites on the substrate). This phenomenon makes it possible to monitor the surface chemical composition during MBE growth. Figure 17 demonstrates the PRS signal variation during growth of GaAs under different As_4 pressure p_{As} conditions. The growth was continued for 10 s using the Ga flux intensity of N_s (cm^2/s). Before opening the Ga effusion cell shutter, the As-stable surface with (2×4) reconstruction [1] was confirmed by RHEED observation. During MBE growth using $p_{As} = 5.3\times10^{-6}$ Torr (uppermost trace in Fig. 17), the PRS signal showed higher intensity than that before and after growth, indicating increased Ga concentration in the growing surface. However, the corresponding RHEED signal showed a distinct specular beam intensity oscillation throughout the entire growth duration (10 s). This result indicates that PRS is not sensitive to structural changes in the growing surface (no relevant PRS signal intensity oscillations could be ob-

 © 1999 COSiW SEP, Warsaw

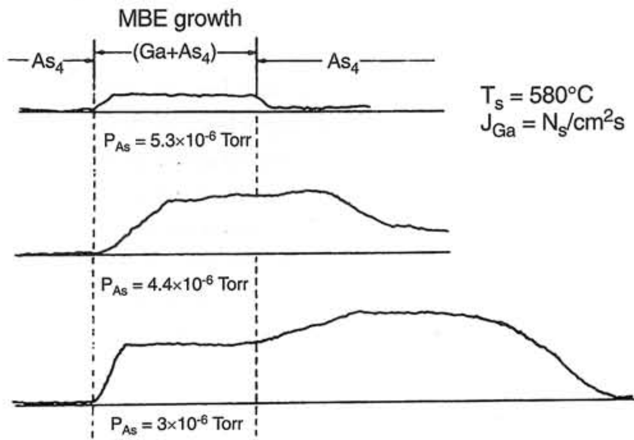

Fig. 17. PRS signal intensity variation during the MBE growth of GaAs. The incident light wavelength was 325 nm (after Ref. 19).

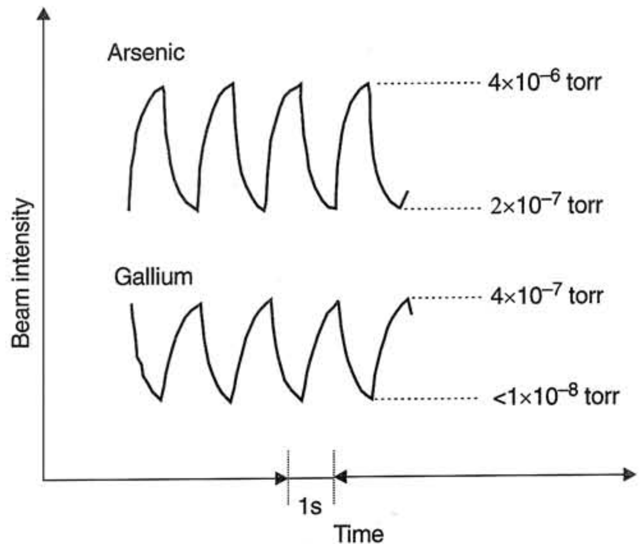

Fig. 18. Beam intensity change for Ga and As_4 species caused by shutter operation characteristic of MEE (after Ref. 1).

served). For the reduced As_4 pressure conditions (lower two traces of Fig. 17) the PRS signal intensity increases and finally saturates. This saturation value corresponds to the intensity of the (001) GaAs surface fully covered with Ga atoms. After saturation, excess Ga adatoms are stored in the form of droplets on the growing surface. Thus, it takes a long time to recover to the original As-stable surface after growing. These low p_{As} conditions [$(4.4$ and $3)\times10^{-6}$ Torr] produce no specular surfaces for the continued growth. In conclusion, the observation of the PRS signal in MBE growth enables optimization of the As flux (As pressure at the surface) when Ga flux is already optimized to the value $J_{Ga} = N_s$ (cm^2/s).

4.2. Application of PRS to migration-enhanced epitaxy

Optimization of the As_4 deposition rate is also possible in migration-enhanced epitaxy (MEE) [19]. In this growth technique the cation atoms (Ga, or Ga and Al, in the cases of epitaxy of GaAs or AlGaAs, respectively) and the relevant anion atoms (As in the cases of GaAs or AlGaAs) are alternately supplied to the GaAs (001) surface to obtain metal-stabilized surface periodically. The typical switching behaviour of As_4 and Ga beam intensity measured by an ionization gauge placed at the substrate holder position is shown in Fig. 18. Bearing in mind the response time of the ionization gauge amplifier, the observed response indicates that the beam intensities change very quickly following the shutter operation. It has been evidenced experimentally, that the MEE growth of GaAs and AlGaAs proceeds in a layer-by-layer manner [1].

Figure 19 indicates the PRS intensity traces for 5-cycle MEE growth of GaAs. The growth rate was fixed to 1 monolayer per cycle [19]. A steady oscillation in the PRS signal intensity (upper trace) was obtained using $p_{As} = 7\times10^{-6}$ Torr. In this case, As_4 deposition was continued for 3 s in each cycle. However, the As-stable surface was recovered within 1 s deposition (see the time needed for the complete intensity drop to the original level in each cycle). When p_{As} was reduced to 3×10^{-6} Torr, the PRS signal intensity drop in the As_4 deposition duration occurred very

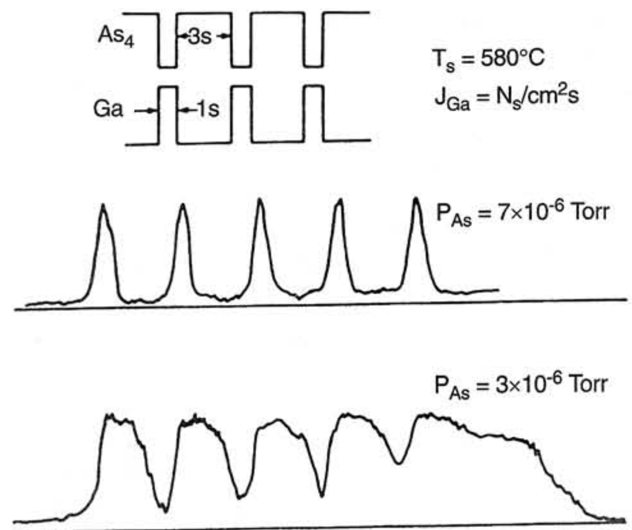

Fig. 19. PRS signal intensity traces observed using light of wavelength equal to 325 nm for 5-cycle MEE growth of GaAs at 580°C. Optimization of As_4 deposition rate can be done (after Ref. 19).

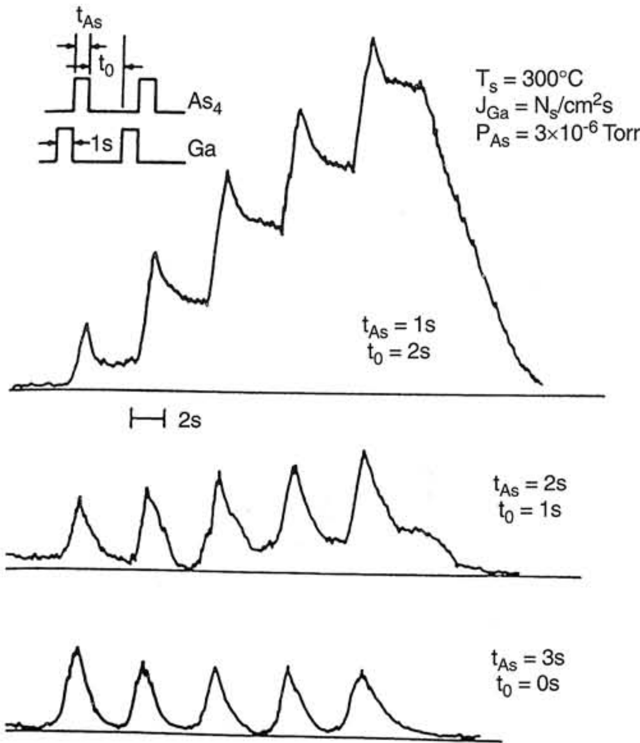

Fig. 20. PRS signal intensity traces of 5-cycle MEE growth of GaAs at 300°C (after Ref. 19).

slowly and incompletely, indicating that excess Ga atoms agglomerate on the growing surface.

The results obtained for a reduced substrate temperature (300°C) are shown in Fig. 20. The deposition sequence is depicted in the inset. In this case, p_{As} was fixed at 3×10^{-6} Torr and the deposition duration was changed for different traces. When the deposition duration is equal to 1 s (upper most trace), no steady oscillation was observed because of insufficient As_4 deposition. Even for the first cycle, no complete recovery to the As-stable surface was obtained. In contrast to the high temperature result (see the lower trace in Fig. 19) the PRS signal intensity grows continuously. This phenomenon implies that no large Ga droplet is formed on the growing surface even when excess Ga atoms are accumulated on the surface Ga layer. Instead, the growing surface is probably covered by higher density but very small Ga droplets at this substrate temperature. By increasing the As_4 deposition duration, stationary PRS oscillation can be achieved as shown in the lower most trace in Fig. 20. From these results, it is very easy to optimise the As_4 deposition rate.

In conclusion, the PRS method proved useful for monitoring surface chemical composition during MBE and fractional layer growth by MEE.

5. Conclusions

On the basis of the large number of papers published currently on different aspects of optical characterization methods, as applied to control of the epitaxial growth techniques [6], one may expect that the nearest future will see an intensification of studies and application areas of these methods, which in short have been discussed in this paper. For reason of keeping this review short, some of important optical techniques have not been included into the scope of this paper. Let us mention as examples: ellipsometry [21], laser light scatterometry [22], and scanning near-field optical microscopy [23]. It has to be emphasised that all optical techniques currently used for control of epitaxy in general, and MBE in the detail, exhibit the following experimentally important features:

(i) they are nondestructive and very sensitive characterization techniques, which nowadays enable the analysis of epitaxial layers with thicknesses on the atomic scale,

(ii) real-time observation of surface processes occurring during the epitaxial growth is possible with the group of the reflectance difference spectroscopies,

(iii) the best prospects for future developments of real-time optical control of MBE growth processes are provided by combination of p-polarized light reflectance spectroscopy, laser interferometry, and laser light scatterometry with the reflectance difference spectroscopy [22].

References

1. M.A. Herman and H. Sitter, *Molecular Beam Epitaxy – Fundamentals and Current Status*, 2nd edition, Springer-Verlag, Berlin, 1996.
2. J. Sadowski and M.A. Herman, "Hard heteroepitaxy of MBE-grown PbTe on off oriented GaAs(100) substrates", *J. Cryst. Growth* **146**, 449 (1995).
3. J. Sadowski, E. Dynowska, K. Regiński, and M.A. Herman, "Hard heteroepitaxy on 2° off-oriented GaAs(100) substrates: The occurrence of (100) and (111) surface orientations in MBE-grown PbTe films", *Cryst. Res. Technol.* **28**, 909 (1993).
4. H. Lüth, *Surfaces and Interfaces of Solid Materials*, 3rd edition, Springer-Verlag, Berlin, 1995.
5. W. Braun, *RHEED Studies of Semiconductor Interfaces During Growth by MBE*, Springer-Verlag, Berlin, 1999.

 © 1999 COSiW SEP, Warsaw

6. G. Bauer and W. Richter (eds.), *Optical Characterization of Epitaxial Semiconductor Layers*, Springer-Verlag, Berlin, 1996.
7. H. Sitter, G.J. Glanner, and M.A. Herman, "Exact determination of the real substrate temperature and film thickness in vacuum epitaxial growth systems by visible laser interferometry", *Vacuum* **46**, 69 (1995).
8. M. Born and E. Wolf, *Principles of Optics*, Sects. 1.5 and 7.6, Pergamon Press, Oxford, 1975.
9. G.J. Glanner, H. Sitter, W. Faschinger, and M.A. Herman, "Evaluation of growth temperature, refractive index, and layer thickness of thin ZnTe, MnTe, and CdTe films by in-situ visible laser interferometry", *Appl. Phys. Lett.* **65**, 2538 (1994).
10. M.A. Herman, A.V. Kozhukhov, and J.T. Sadowski, "The MBE temperature window for $Cd_{1-x}Zn_xTe$ ($0 \le x \le 1$) compounds grown on 2°-off oriented GaAs(100) substrates", *J. Cryst. Growth* **174**, 768 (1997).
11. D.J. Eaglesham, "Semiconductor molecular beam epitaxy at low temperatures", *J. Appl. Phys.* **77**, 3597 (1995).
12. J.Y. Tsao, *Materials Fundamentals of MBE*, Chap. 3, Academic Press, Boston, 1993.
13. D.A. Aspnes, "Analysis and control of semiconductor crystal growth with reflectance difference spectroscopy and spectroellipsometry", *Proc. SPIE* **1361**, 551 (1990).
14. G. Paulsson, K. Deppert, S. Jeppesen, J. Jönsson, L. Samuelson, and P. Schmidt, "Reflectance-difference detection of growth oscillations", *J. Cryst. Growth* **105**, 312 (1990).
15. D.E. Aspnes, W.E. Quinn, S. Gregory, "Real-time diagnostics for epitaxial growth", *J. Vac. Sci. Technol.* A **9**, 870 (1991).
16. D.E. Aspnes, J.P. Harbison, A.A. Studna, and L.T. Florez, "Optical-reflectance and electron-diffraction studies of MBE growth transients on GaAs(001)", *Phys. Rev. Lett.* **59**, 1687 (1987).
17. J.P. Harbison, D.E. Aspnes, A.A. Studna, L.T. Florez, and M.K. Kelly, "Oscillations in the optical response of (001) GaAs and AlGaAs surfaces during crystal growth by MBE", *Appl. Phys. Lett.* **52**, 2046 (1988).
18. N. Kobayashi and Y. Horikoshi, "Optical investigation on the growth process of GaAs during Migration-Enhanced Epitaxy", *Jpn. J. Appl. Phys.* **28**, L 1880 (1989).
19. Y. Horikoshi, M. Kawashima, and N. Kobayashi, "Optical investigation of GaAs growth process in MBE and MEE", *J. Cryst. Growth* **111**, 200 (1991).
20. R. Eryigit, P.K. Marschel, and I.P. Herman. "Use of surface photoabsorption to analyse the optical response of GaAs(001) surfaces", *J. Vac. Sci. Technol.* A **15**, 138 (1997).
21. U. Rossow and W. Richter, "Spectroscopic ellipsometry", Ch. 3 in [Ref. 6].
22. K.J. Bachmann, C. Höpfner, N. Sukidi, A.E. Miller, C. Harris, D.E. Aspnes, N.A. Dietz, H.T. Tran, S. Beeler, K. Ito, H.T. Banks, and U. Rossow, "Molecular layer epitaxy by real-time optical process monitoring", *Appl. Surf. Sci.* **112**, 38 (1997).
23. M.A. Herman, "Scanning near-field optical microscopy", *Opto-Electronics Rev.* **5**, 295 (1997).